Neda Karami Mohammadi
Department of Mechanical Engineering,
University of Wisconsin Madison,
Madison, WI 53706
e-mail: nkaramim@yahoo.com

Pavel I. Galich
Department of Aerospace Engineering,
Technion—Israel Institute of Technology,
Haifa 32000, Israel;
Department of Materials Science and
NanoEngineering,
Rice University,
Houston, TX 77005
e-mail: galich@technion.ac.il

Anastasia O. Krushynska
Engineering and Technology Institute Groningen
(ENTEG),
Faculty of Science and Engineering,
University of Groningen,
Groningen 9747AG, The Netherlands
e-mail: akrushynska@gmail.com

Stephan Rudykh[1]
Department of Mechanical Engineering,
University of Wisconsin Madison,
Madison, WI 53706
e-mail: rudykh@wisc.edu

Soft Magnetoactive Laminates: Large Deformations, Transverse Elastic Waves and Band Gaps Tunability by a Magnetic Field

We investigate the behavior of soft magnetoactive periodic laminates under remotely applied magnetic field. We derive explicit formulae for the induced deformation due to magnetic excitation of the laminates with hyperelastic magnetoactive phases. Next, we obtain the closed-form formulae for the velocities of long transverse waves. We show the dependence of the wave velocity on the applied magnetic intensity and induced strains, as well as on the wave propagation direction. Based on the long wave analysis, we derive closed-form formulae for the critical magnetic field corresponding to the loss of macroscopic stability. Finally, we analyze the transverse wave band gaps appearing in magnetoactive laminates in the direction normal to the layers. We illustrate the band gap tunability—width and position—by magnetically induced deformation.
[DOI: 10.1115/1.4044497]

Keywords: magnetoactive materials, laminates, transverse waves, large deformations, band gaps, elasticity, mechanical properties of materials, micromechanics, wave propagation

1 Introduction

Magnetoactive elastomers (MAE) can change their size and material properties in response to a remotely applied magnetic field. Typically, these soft active materials are composed of magnetizable particles (such as iron, nickel, or Terfenol-D) dispersed in a polymer matrix [1,2]. An external magnetic field magnetizes the particles, resulting in modification of the mechanical properties and deformation of the soft composites. The remote and reversible principle of actuation and properties modification naturally lends these active materials to a large variety of applications, such as variable-stiffness devices [3–5], tunable vibration absorbers [6–8], damping components [9,10], noise barriers [11,12], sensors [13,14], actuators [15–17], bio-medicine [18], and soft robotics [19,20] among others. In this paper, we focus on the applications of MAEs for remote control and manipulation of elastic waves.

The development of the research on wave propagation in magnetoelastic materials (up to 1981) is summarized by Maugin [21], along with providing the governing equations for magnetoelastic waves in finitely strained materials. Succeeding works on wave phenomena in magnetoelastic materials have analyzed nonlinear surface waves [22,23] and inhomogeneous plane waves [24]. Destrade and Ogden [25] have generalized the analysis of the infinitesimal waves in the finitely strained magnetoelastic solids in a magnetic field. Following this noteworthy contribution, Saxena and Ogden have investigated Rayleigh-type surface waves [26] and Love-type waves [27] propagating in a finitely deformed isotropic and layered half-spaces of an incompressible non-conducting magnetoelastic solids immersed into a magnetic field, respectively.

Here, we consider transverse wave propagation in finitely deformed bi-phase periodic magnetoelastic layered composites in the presence of a magnetic field. Following the studies on elastic waves in purely mechanical hyperelastic laminates [28] and in finitely strained dielectric elastomer laminates in the electric field [29], we consider small amplitude transverse waves in the magnetoelastic layered medium with two isotropic alternating magnetoelastic materials. We exploit a *micromechanics*-based technique [30] and derive the closed-form formulas for the velocities of long (wavelength ≫ period of the laminate) transverse waves. The explicit formulas are given for a general propagation direction. Based on our long wave analysis, the explicit expressions for the critical magnetic field and stretch for the loss of stability are derived. Additionally, we consider the case of magnetodeformation (often referred to as magnetostriction in the literature [1,2,31–33]), when we induce deformation by a magnetic field applied normally to the layers and derive explicit relation for the induced stretch. These results can be used for verification of numerical approaches for modeling of the magnetoelastic materials [34–36]. Finally, we derive the dispersion relation for the transverse waves propagating normally to the layers under the finite strains induced by a magnetic field.

2 Overview of Nonlinear Magnetoelasticity

Consider a magnetoelastic solid occupying Ω_0 and Ω_t domains in the undeformed and deformed configurations, respectively. The deformation gradient is $\mathbf{F}(\mathbf{X}, t) = \partial \mathbf{x}(\mathbf{X}, t)/\partial \mathbf{X}$, with $\mathbf{X}$ and $\mathbf{x}$ are position vectors in the undeformed and deformed states. In this paper, we examine *incompressible* solids, so that $J \equiv \det \mathbf{F} = 1$.

We follow the work by Dorfmann and Ogden [37] and consider the quasi-magnetostatic approximation, assuming that there are no electric fields nor free body charges and currents. The magnetostatics equations in the deformed state are

$$\operatorname{div} \mathbf{B} = 0 \text{ and } \operatorname{curl} \mathbf{H} = \mathbf{0} \tag{1}$$

where $\mathbf{B}$ is the magnetic induction and $\mathbf{H}$ is the magnetic intensity in the deformed configuration. Here and thereafter, the first letters of the differential operators indicate either it is taken in the reference

[1]Corresponding author.

Contributed by the Applied Mechanics Division of ASME for publication in the Journal of Applied Mechanics. Manuscript received May 9, 2019; final manuscript received August 2, 2019; published online September 3, 2019. Assoc. Editor: Francois Barthelat.

(capital first letter) or in the current (low-case fist letter) configurations. The magnetostatics equations in the undeformed configuration are

$$\text{Div}\ \mathbf{B}_L = 0 \quad \text{and} \quad \text{Curl}\ \mathbf{H}_L = \mathbf{0} \tag{2}$$

where

$$\mathbf{B}_L = \mathbf{F}^{-1}\cdot\mathbf{B} \quad \text{and} \quad \mathbf{H}_L = \mathbf{F}^{T}\cdot\mathbf{H} \tag{3}$$

are the Lagrangian magnetic induction and magnetic intensity, respectively.

Assuming that there are no body forces, and the deformation is applied quasi-statically, we can write the equations of motion as

$$\text{div}\ \boldsymbol{\sigma} = \mathbf{0} \tag{4}$$

Note that $\boldsymbol{\sigma}$ includes the mechanical and magnetic stresses and is referred to as the *total* Cauchy stress tensor; the total stress tensor is symmetric, namely, $\boldsymbol{\sigma}=\boldsymbol{\sigma}^T$. Equation (4) can be transformed into the corresponding form in the undeformed configuration

$$\text{Div}\ \mathbf{P} = \mathbf{0} \tag{5}$$

where $\mathbf{P}$ is the first Piola-Kirchhoff *total* stress tensor related to $\boldsymbol{\sigma}$ via the following relations for an incompressible material

$$\mathbf{P} = \boldsymbol{\sigma}\cdot\mathbf{F}^{-T} \tag{6}$$

Consider an energy-density scalar-valued function $\psi(\mathbf{F}, \mathbf{B}_L)$ such that

$$\mathbf{P} = \frac{\partial\psi}{\partial\mathbf{F}} - p\mathbf{F}^{-T} \quad \text{and} \quad \mathbf{H}_L = \frac{\partial\psi}{\partial\mathbf{B}_L} \tag{7}$$

Due to the incompressibility constraint, the unknown scalar p is introduced. By defining the tensors of magnetoelastic moduli as

$$\mathbb{C}_0 = \frac{\partial^2\psi}{\partial\mathbf{F}\partial\mathbf{F}}, \quad \mathcal{B}_0 = \frac{\partial^2\psi}{\partial\mathbf{F}\partial\mathbf{B}_L}, \quad \text{and} \quad \mathbf{M}_0 = \frac{\partial^2\psi}{\partial\mathbf{B}_L\partial\mathbf{B}_L} \tag{8}$$

the linearized (or incremental) constitutive equations can be written as

$$\begin{aligned}\dot{\mathbf{P}} &= \mathbb{C}_0 : \dot{\mathbf{F}} + p\mathbf{F}^{-T}\cdot\dot{\mathbf{F}}^{T}\cdot\mathbf{F}^{-T} - \dot{p}\mathbf{F}^{-T} + \mathcal{B}_0\cdot\dot{\mathbf{B}}_L \quad \text{and}\\ \dot{\mathbf{H}}_L &= \dot{\mathbf{F}} : \mathcal{B}_0 + \mathbf{M}_0\cdot\dot{\mathbf{B}}_L\end{aligned} \tag{9}$$

where $\dot{\mathbf{F}}$, $\dot{p}$, $\dot{\mathbf{B}}_L$, and $\dot{\mathbf{H}}_L$ are the incremental changes in $\mathbf{F}$, p, $\mathbf{B}_L$, and $\mathbf{H}_L$, respectively.

By introducing the counterparts of $\dot{\mathbf{B}}_L$, $\dot{\mathbf{H}}_L$, and $\dot{\mathbf{P}}$ in the frame of the updated Lagrangian formulation, namely

$$\dot{\mathbf{B}}_{L\star} = \mathbf{F}\cdot\dot{\mathbf{B}}_L, \quad \dot{\mathbf{H}}_{L\star} = \mathbf{F}^{-T}\cdot\dot{\mathbf{H}}_L, \quad \text{and} \quad \dot{\mathbf{P}}_\star = \dot{\mathbf{P}}\cdot\mathbf{F}^{T} \tag{10}$$

we can write the corresponding equations for infinitesimal motions ("small on large") as

$$\text{div}\,\dot{\mathbf{B}}_{L\star} = 0, \quad \text{curl}\,\dot{\mathbf{H}}_{L\star} = \mathbf{0}, \quad \text{and} \quad \text{div}\,\dot{\mathbf{P}}_\star = \rho\dot{\mathbf{x}}_{,tt} \tag{11}$$

where ρ is the density. Next, with the updated tensors of elastic moduli defined as

$$\begin{aligned}&\mathbb{C}_{irks} = \mathbb{C}_{0ijkl}F_{rj}F_{sl}, \quad \mathcal{B}_{irk} = \mathcal{B}_{0ijm}F_{rj}F^{-1}_{mk}, \quad \text{and}\\ &\mathbf{M} = \mathbf{F}^{-T}\cdot\mathbf{M}_0\cdot\mathbf{F}^{-1}\end{aligned} \tag{12}$$

the linearized constitutive law (Eq. (9)) can be rewritten as

$$\begin{aligned}\dot{\mathbf{P}}_\star &= \mathbb{C} : \mathbf{U} + p\mathbf{U}^T - \dot{p}\mathbf{I} + \mathcal{B}\cdot\dot{\mathbf{B}}_{L\star} \quad \text{and}\\ \dot{\mathbf{H}}_{L\star} &= \mathbf{U} : \mathcal{B} + \mathbf{M}\cdot\dot{\mathbf{B}}_{L\star}\end{aligned} \tag{13}$$

where we have used $\dot{\mathbf{x}} = \mathbf{u}$, $\mathbf{U} = \text{grad}\,\mathbf{u} = \dot{\mathbf{F}}\cdot\mathbf{F}^{-1}$ together with the incompressibility constraint

$$\text{tr}\mathbf{U} \equiv \text{div}\,\mathbf{u} = 0 \tag{14}$$

Next, we follow Destrade and Ogden [25] and look for a solution for Eq. (11) in the form of plane waves, namely

$$\mathbf{u} = \mathbf{g}\,f(\mathbf{n}\cdot\mathbf{x} - ct), \quad \dot{\mathbf{B}}_{L\star} = \mathbf{h}\,h(\mathbf{n}\cdot\mathbf{x} - ct), \quad \text{and} \quad \dot{p} = \Pi(\mathbf{n}\cdot\mathbf{x} - ct) \tag{15}$$

where f, h, and Π are sufficiently smooth function, $\mathbf{n}$ is the direction of wave propagation, c is the velocity, and $\mathbf{g}$ and $\mathbf{h}$ are the corresponding polarization vectors. Inserting Eqs. (13) and (15) into Eqs. (11) and (14), we obtain the following eigenvalue problem for the generalized acoustic tensor $\hat{\mathbf{A}}$ for an incompressible magnetoelastic solid:

$$\hat{\mathbf{A}}\cdot\mathbf{g} = \rho c^2\mathbf{g} \quad \text{and} \quad \mathbf{g}\cdot\mathbf{n} = 0 \tag{16}$$

The generalized acoustic tensor is given as [25]

$$\hat{\mathbf{A}} = \hat{\mathbf{Q}} - \frac{2}{(\text{tr}\hat{\mathbf{M}})^2 - \text{tr}\hat{\mathbf{M}}^2}\hat{\mathbf{Z}}\cdot\left((\text{tr}\hat{\mathbf{M}})\hat{\mathbf{I}} - \hat{\mathbf{M}}\right)\cdot\hat{\mathbf{Z}}^T \tag{17}$$

where $\hat{\mathbf{I}} = \mathbf{I} - \mathbf{n}\otimes\mathbf{n}$ is the projection tensor, $\hat{\mathbf{M}} = \hat{\mathbf{I}}\cdot\mathbf{M}\cdot\hat{\mathbf{I}}$, $\hat{\mathbf{Q}} = \hat{\mathbf{I}}\cdot\mathbf{Q}\cdot\hat{\mathbf{I}}$, $\hat{\mathbf{Z}} = \hat{\mathbf{I}}\cdot\mathbf{Z}\cdot\hat{\mathbf{I}}$, $Q_{ik} = \mathbb{C}_{ijkl}\,n_j n_l$, and $\mathbf{Z} = \mathbf{n}\cdot\mathcal{B}$. The eigenvalues of the generalized acoustic tensor $\hat{\mathbf{A}}$ define the velocities of the plane waves propagating in a magnetoelastic solid.

3 Results and Discussion

We examine magnetoelastic layered materials (schematically shown in Fig. 1(*a*)) with two isotropic incompressible constituents with volume fractions $v^{(1)}$ and $v^{(2)} = 1 - v^{(1)}$; thus, the alternating layer thicknesses are $L^{(1)} = v^{(1)}L$ and $L^{(2)} = v^{(2)}L$, and L is the period of the undeformed layered material. Here, we denote the parameters of the corresponding constituents as $(\bullet)^{(1)}$ and $(\bullet)^{(2)}$.

Magnetic excitation results in deformation of MAEs (as shown in Fig. 1(*b*)), so that the thicknesses become

$$l^{(1)} = \lambda_2^{(1)}L^{(1)}, \quad l^{(2)} = \lambda_2^{(2)}L^{(2)}, \quad \text{and} \quad l = \bar{\lambda}_2 L \tag{18}$$

where $\lambda_2^{(1)}$ and $\lambda_2^{(2)}$ are the phase stretch ratios in the direction $\mathbf{e}_2$ and $\bar{\lambda}_2 = v^{(1)}\lambda_2^{(1)} + v^{(2)}\lambda_2^{(2)}$ is the corresponding average stretch ratio.

The average deformation gradient $\bar{\mathbf{F}}$ and Lagrangian magnetic induction $\bar{\mathbf{B}}_L$ represent the macroscopically applied magnetomechanical loads defined as

$$\bar{\mathbf{F}} = v^{(1)}\mathbf{F}^{(1)} + v^{(2)}\mathbf{F}^{(2)} \quad \text{and} \quad \bar{\mathbf{B}}_L = v^{(1)}\mathbf{B}_L^{(1)} + v^{(2)}\mathbf{B}_L^{(2)} \tag{19}$$

The displacements continuity condition at the layer interface yields

$$\left(\mathbf{F}^{(1)} - \mathbf{F}^{(2)}\right)\cdot\mathbf{s} = \mathbf{0} \tag{20}$$

where $\mathbf{s}$ is a unit vector normal to $\mathbf{m}$, which is a unit vector denoting the initial lamination direction. The tractions continuity condition results in

$$\left(\mathbf{P}^{(1)} - \mathbf{P}^{(2)}\right)\cdot\mathbf{m} = \mathbf{0} \tag{21}$$

The corresponding interface conditions for $\mathbf{B}_L$ and $\mathbf{H}_L$ are

$$\left(\mathbf{B}_L^{(1)} - \mathbf{B}_L^{(2)}\right)\cdot\mathbf{m} = 0 \quad \text{and} \quad \left(\mathbf{H}_L^{(1)} - \mathbf{H}_L^{(2)}\right)\times\mathbf{m} = \mathbf{0} \tag{22}$$

The interface conditions Eqs. (21) and (22) can be written in the deformed state as

$$\begin{aligned}&\left(\boldsymbol{\sigma}^{(1)} - \boldsymbol{\sigma}^{(2)}\right)\cdot\mathbf{m} = \mathbf{0}, \quad \left(\mathbf{B}^{(1)} - \mathbf{B}^{(2)}\right)\cdot\mathbf{m} = 0, \quad \text{and}\\ &\left(\mathbf{H}^{(1)} - \mathbf{H}^{(2)}\right)\times\mathbf{m} = \mathbf{0}\end{aligned} \tag{23}$$

3.1 Magnetodeformation. Consider the laminates with the phases defined by the following energy-density function (EDF) for isotropic *incompressible* magnetoelastic materials

$$\psi^{(\xi)}(I_1^{(\xi)}, I_5^{(\xi)}) = \psi_{elas}^{(\xi)}(I_1^{(\xi)}) + \frac{1}{2\,\mu^{(\xi)}}I_5^{(\xi)} \tag{24}$$

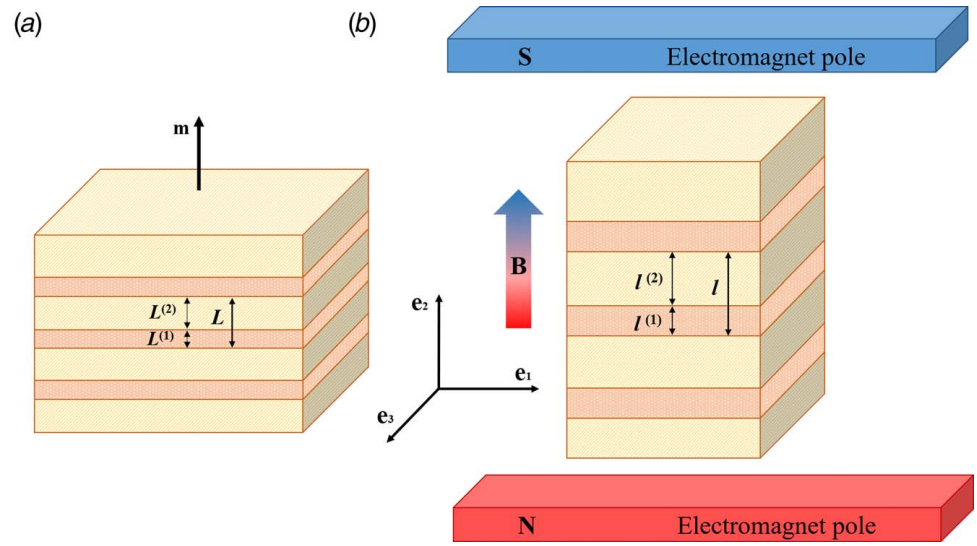

Fig. 1 MAE laminates in (*a*) the undeformed and (*b*) magnetically deformed states

where $\psi^{(\xi)}_{elas}(I^{(\xi)}_1)$ represents the mechanical part of the total EDF, $\mathbf{C}$ is the right Cauchy-Green deformation tensor, $I_1 = \mathrm{tr}\mathbf{C} = \mathbf{F} : \mathbf{F}$ is its first invariant, $I_5 = \mathbf{B}_L \cdot \mathbf{C} \cdot \mathbf{B}_L$ is the invariant accounting for the magnetomechanical coupling, and $\mu^{(\xi)}$ is the magnetic permeability. First, consider the EDF (24) with neo-Hookean elastic part, namely

$$\psi^{(\xi)}_{elas}(I^{(\xi)}_1) = \frac{G^{(\xi)}}{2}\left(I^{(\xi)}_1 - 3\right) \tag{25}$$

where $G^{(\xi)}$ is the shear modulus. For incompressible neo-Hookean magnetoelastic laminates, an exact solution can be obtained [30]. The solution can be used for constructing the following effective EDF

$$\psi(\bar{\mathbf{F}}, \bar{\mathbf{B}}_L) = \tilde{\psi}_{elas}(\bar{\mathbf{F}}) + \tilde{\psi}_c(\bar{\mathbf{F}}, \bar{\mathbf{B}}_L) \tag{26}$$

where the elastic part of the EDF is

$$\tilde{\psi}_{elas}(\bar{\mathbf{F}}) = \frac{\bar{G}}{2}\left(\bar{\mathbf{F}} : \bar{\mathbf{F}} - 3\right) - \frac{\bar{G} - \check{G}}{2}\left(\mathbf{m} \cdot \bar{\mathbf{C}} \cdot \mathbf{m} - \frac{1}{\mathbf{m} \cdot \bar{\mathbf{C}}^{-1} \cdot \mathbf{m}}\right) \tag{27}$$

where $\bar{\mathbf{C}} = \bar{\mathbf{F}}^T \cdot \bar{\mathbf{F}}$ and the effective shear moduli are defined as $\bar{G} = v^{(1)}G^{(1)} + v^{(2)}G^{(2)}$ and $\check{G} = \left(v^{(1)}/G^{(1)} + v^{(2)}/G^{(2)}\right)^{-1}$. The magnetoelastic coupled term of the EDF is

$$\tilde{\psi}_c(\bar{\mathbf{F}}, \bar{\mathbf{B}}_L) = \frac{1}{2\,\bar{\mu}}\ \bar{\mathbf{B}}_L \cdot \bar{\mathbf{C}} \cdot \bar{\mathbf{B}}_L + \frac{1}{2}\left(\frac{1}{\check{\mu}} - \frac{1}{\bar{\mu}}\right)\frac{\left(\bar{\mathbf{B}}_L \cdot \mathbf{m}\right)^2}{\mathbf{m} \cdot \bar{\mathbf{C}}^{-1} \cdot \mathbf{m}} \tag{28}$$

where the effective permeability moduli are $\bar{\mu} = v^{(1)}\mu^{(1)} + v^{(2)}\mu^{(2)}$ and $\check{\mu} = \left(v^{(1)}/\mu^{(1)} + v^{(2)}/\mu^{(2)}\right)^{-1}$.

Next, we examine the case of the magnetoelastic laminates deforming due to a magnetic field applied normally to the layers, as defined by the following setting:

$$\mathbf{m} = \mathbf{e}_2, \quad \bar{\mathbf{B}}_L = B_L\sqrt{\bar{G}\check{\mu}}\,\mathbf{e}_2, \quad \text{and} \quad \bar{\boldsymbol{\sigma}} = v^{(1)}\boldsymbol{\sigma}^{(1)} + v^{(2)}\boldsymbol{\sigma}^{(2)} = \boldsymbol{\sigma}^*_M \tag{29}$$

where

$$\boldsymbol{\sigma}^*_M = \frac{1}{\mu_0}\left(\mathbf{B}^* \otimes \mathbf{B}^* - \frac{1}{2}\left(\mathbf{B}^* \cdot \mathbf{B}^*\right)\mathbf{I}\right) \tag{30}$$

is the Maxwell stress outside the laminate, μ_0 is the vacuum magnetic permeability, and $\mathbf{B}^* = B_L\sqrt{\bar{G}\check{\mu}}\ \mathbf{e}_2$ is the magnetic induction outside the laminate. Note that B_L denotes the nondimensional (or normalized) magnetic induction, while its physical value (measured in Tesla (T)) can be obtained by multiplying the normalized value by $\sqrt{\bar{G}\check{\mu}}$. By making use of the incompressibility condition along with the in-plane symmetry ($\langle \mathbf{e}_1, \mathbf{e}_3 \rangle$) and the interface displacement continuity condition (Eq. (20)), we can write the average deformation gradient as

$$\bar{\mathbf{F}} = \lambda\mathbf{e}_2 \otimes \mathbf{e}_2 + \lambda^{-1/2}(\mathbf{I} - \mathbf{e}_2 \otimes \mathbf{e}_2) \tag{31}$$

The Cauchy stress and magnetic field in the phases are

$$\boldsymbol{\sigma}^{(\xi)} = G^{(\xi)}\mathbf{b}^{(\xi)} + (\mu^{(\xi)})^{-1}\mathbf{B}^{(\xi)} \otimes \mathbf{B}^{(\xi)} - p^{(\xi)}\mathbf{I} \quad \text{and} \quad \mathbf{H}^{(\xi)} = \mathbf{B}^{(\xi)}/\mu^{(\xi)} \tag{32}$$

Since we consider the case for which $\mathbf{B}^{(\xi)} = B_2\,\mathbf{e}_2 = \lambda B_L\sqrt{\bar{G}\check{\mu}}\,\mathbf{e}_2$ and $\mathbf{b}^{(\xi)} = \lambda^2\,\mathbf{e}_2 \otimes \mathbf{e}_2 + \lambda^{-1}(\mathbf{I} - \mathbf{e}_2 \otimes \mathbf{e}_2)$, then the stress components are

$$\begin{aligned} \sigma^{(\xi)}_{11} = \sigma^{(\xi)}_{33} &= G^{(\xi)}\lambda^{-1} - p^{(\xi)} \quad \text{and} \\ \sigma^{(\xi)}_{22} &= G^{(\xi)}\lambda^2 + (\mu^{(\xi)})^{-1}\bar{G}\,\check{\mu}\,\lambda^2 B^2_L - p^{(\xi)} \end{aligned} \tag{33}$$

From the traction continuity condition for the layer interfaces Eq. $(23)_1$, and for the laminate-outer-space continuity condition Eq. $(29)_3$, we obtain

$$\sigma^{(1)}_{22} = \sigma^{(2)}_{22} = \frac{1}{2}\bar{G}\,\check{\mu}_r\,B^2_L \quad \text{and} \quad v^{(1)}\sigma^{(1)}_{11} + v^{(2)}\sigma^{(2)}_{11} = -\frac{1}{2}\bar{G}\,\check{\mu}_r\,B^2_L \tag{34}$$

where $\check{\mu}_r = \left(v^{(1)}/\mu^{(1)}_r + v^{(2)}/\mu^{(2)}_r\right)^{-1}$ is the weighted harmonic mean of relative permeability ($\mu^{(\xi)}_r = \mu^{(\xi)}/\mu_0$). Equation (34) produces the relations between field intensity B_L and induced stretch λ as

$$B^2_L = \frac{\lambda^3 - 1}{\lambda\left(\check{\mu}_r - \lambda^2\right)} \tag{35}$$

the results can be also written for the nondimensional Eulerian magnetic induction, namely,

$$B^2 = \frac{\lambda\left(\lambda^3 - 1\right)}{\check{\mu}_r - \lambda^2} \tag{36}$$

Due to the choice of the normalization, the relationship (35) and (36) are independent of the shear moduli. For magnetoactive laminates $\check{\mu}_r > 1$ (otherwise, the laminate is magnetically inactive), thus, Eq. (36) yields

$$1 \le \lambda < \sqrt{\check{\mu}_r} \tag{37}$$

Hence, a magnetic field applied normally to the layers results in contraction of the laminates along the layers. Moreover, the

induced stretch is bounded by the certain value defined by the magnetic properties of the constituents. We note that under certain magnetomechanical loading, the laminates may experience magnetoelastic instabilities [30,38]; a more detailed discussion of the magnetoelastic instability phenomenon in the magnetoactive laminates is given in the Sec. 3.2.2.

To account for stiffening phenomena due to, e.g., the finite extensibility of polymer chains [39], we consider the Gent model [40] for the phases

$$\psi_{elas}^{(\xi)}(F^{(\xi)}) = -\frac{\mu^{(\xi)} J_m^{(\xi)}}{2} \ln\left(1 - \frac{I_1^{(\xi)} - 3}{J_m^{(\xi)}}\right) \tag{38}$$

where $J_m^{(\xi)}$ is the locking parameter; recall that in the limit of $(I_1^{(\xi)} - 3) \to J_m^{(\xi)}$, the EDF increases drastically. In MAEs laminates with magnetoelastic Gent phases immersed into a magnetic field normal to the layers (according to Eq. (29)), the stretch and Lagrangian magnetic induction are related via

$$B_L{}^2 = \frac{\lambda^3 - 1}{\bar{G}\,\lambda\,(\check{\mu}_r - \lambda^2)}\left[G^{(1)}\,\nu^{(1)}\,\eta^{(1)} + G^{(2)}\,\nu^{(2)}\,\eta^{(2)}\right] \tag{39}$$

where $\eta^{(\xi)} = J_m{}^{(\xi)}\left(3 + J_m{}^{(\xi)} - \lambda^2 - 2\lambda^{-1}\right)^{-1}$. If both phases are characterized by identical locking parameter $J_m{}^{(1)} = J_m{}^{(2)} = J_m$, Eq. (39) reduces to

$$B_L{}^2 = \frac{\lambda^2 - \lambda^{-1}}{\check{\mu}_r - \lambda^2}\left(\frac{J_m}{3 + J_m - \lambda^2 - 2\lambda^{-1}}\right) \tag{40}$$

In terms of Eulerian magnetic induction, Eq. (40) reads as

$$B^2 = \frac{\lambda\left(\lambda^3 - 1\right)}{\check{\mu}_r - \lambda^2}\left(\frac{J_m}{3 + J_m - \lambda^2 - 2\lambda^{-1}}\right) \tag{41}$$

Figure 2 illustrates the results of Eqs. (36) and (41) showing the induced stretch as the function of the dimensionless Eulerian magnetic induction for the neo-Hookean (solid curve) and Gent laminates with $\nu^{(1)} = 0.2$, $\mu_r^{(1)}/\mu_r^{(2)} = 1.5$, and $J_m = 0.1$ (dashed curve) and $J_m = 0.2$ (dashed-dotted curve).

Next, we illustrate the dependence of the magnetodeformation (or magnetostriction) on the phase volume fraction in Fig. 3 showing the variations of induced stretch versus volume fraction $\nu^{(1)}$ for MAE composites with (*a*) Gent with $J_m = 0.1$ and (*b*) neo-Hookean magnetoactive phases. The results are shown for two different ratios of the relative permeability of $\mu_r^{(1)}/\mu_r^{(2)} = 1.5$ and 5

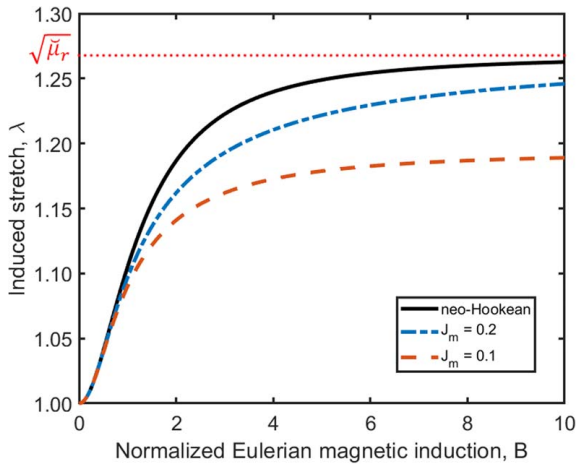

Fig. 2 Induced stretch versus nondimensional Eulerian magnetic induction in neo-Hookean (solid curve) and Gent laminates with $J_m = 0.1$ (dashed curve) and $J_m = 0.2$ (dashed-dotted curve) and $\nu^{(1)} = 0.2$, $\mu_r^{(1)}/\mu_r^{(2)} = 1.5$, and $\mu_r^{(2)} = 1.5$

when $\mu_r^{(2)} = 1.5$. The dotted, dashed, and solid curves correspond to the normalized Eulerian magnetic induction of $B = 2$, 4, and 6, respectively. As expected, an increase in the volume fraction of $\nu^{(1)}$ (the layers with higher relative permeability) leads to an increase in the induced stretch λ in the MAE composites. Figure 3(*b*) illustrates the influence of the stiffening effect on magnetodeformation (or magnetostriction) as compared with the results for neo-Hookean MAE composites shown in Fig. 3(*a*).

3.2 Transverse Waves in Magnetoelastic Laminates Under Magnetomechanical Loads: Long Waves.

The magnetoelastic acoustic tensor (Eq. (17)) for the effective EDF (Eq. (26)) can be written as

$$\hat{\mathbf{A}}(\mathbf{n}, \bar{\mathbf{F}}, \bar{\mathbf{B}}_L) = A_1\hat{\mathbf{I}} + A_2\left(\hat{\mathbf{I}}\cdot\bar{\mathbf{F}}^{-T}\cdot\mathbf{m}\right)\otimes\left(\hat{\mathbf{I}}\cdot\bar{\mathbf{F}}^{-T}\cdot\mathbf{m}\right) \tag{42}$$

where

$$A_1 = \bar{G}\left(\mathbf{n}\cdot\bar{\mathbf{b}}\cdot\mathbf{n}\right) + \left(\check{G} - \bar{G}\right)\left(\mathbf{n}\cdot\bar{\mathbf{F}}\cdot\mathbf{m}\right)^2 \tag{43}$$

and

$$A_2 = \frac{\bar{G} - \check{G}}{\alpha^2}\left(\frac{4\beta^2}{\alpha} - 1\right) - \left(\frac{1}{\check{\mu}} - \frac{1}{\bar{\mu}}\right)\left(\frac{\left(\bar{\mathbf{B}}_L\cdot\mathbf{m}\right)^2}{\alpha^2} - \frac{4}{\gamma} \times\left(\frac{\left(\bar{\mathbf{B}}_L\cdot\mathbf{m}\right)^2\beta^2}{\alpha^2} + \frac{1}{4}\left(\mathbf{n}\cdot\bar{\mathbf{F}}\cdot\bar{\mathbf{B}}_L\right)^2 - \frac{\left(\bar{\mathbf{B}}_L\cdot\mathbf{m}\right)\left(\mathbf{n}\cdot\bar{\mathbf{F}}\cdot\bar{\mathbf{B}}_L\right)\beta}{\alpha}\right)\right) \tag{44}$$

where $\bar{\mathbf{b}} = \bar{\mathbf{F}}\cdot\bar{\mathbf{F}}^T$, $\alpha = \mathbf{m}\cdot\bar{\mathbf{C}}^{-1}\cdot\mathbf{m}$, $\beta = \mathbf{n}\cdot\bar{\mathbf{F}}^{-T}\cdot\mathbf{m}$, and $\gamma = \alpha\,\bar{\mu}/\check{\mu} + \beta^2\left(1 - \bar{\mu}/\check{\mu}\right)$. The eigenvalues of the magnetoelastic acoustic tensor (Eq. (42)) are

$$a_1 = A_1 \quad \text{and} \quad a_2 = A_1 + A_2\left(\alpha - \beta^2\right) \tag{45}$$

The eigenvalues define the values of the transverse wave velocities, namely,

$$\bar{c}_1 = \sqrt{a_1/\bar{\rho}} \quad \text{and} \quad \bar{c}_2 = \sqrt{a_2/\bar{\rho}} \tag{46}$$

where $\bar{\rho} = \nu^{(1)}\rho^{(1)} + \nu^{(2)}\rho^{(2)}$. We note that the first wave velocity $\bar{c}_1$ does not depend on magnetic field, and the expression is the same as for the transverse wave velocity in purely elastic laminates without a magnetic field [28]. The second velocity $\bar{c}_2$, however, depends on the magnetic field.

Next, we specify the results for the magnetically induced deformation gradient (31).

3.2.1 Transverse Waves Traveling Perpendicularly to the Layers. Consider the propagation direction *perpendicular* to the layers ($\mathbf{n} = \mathbf{e}_2$) as schematically shown in Fig. 4(*a*). For this special case, the velocities simplify to

$$\bar{c} = \bar{c}_1 = \bar{c}_2 = \lambda\sqrt{\check{G}/\bar{\rho}} \tag{47}$$

The velocities are identical and explicitly independent of a magnetic field; the external excitation influences the velocities only through the induced stretch $\lambda = \lambda(B_L)$.

3.2.2 Transverse Waves Travelling Parallel to the Layers. Consider the propagation *along* the layers ($\mathbf{n} = \mathbf{e}_1$) as schematically shown in Fig. 4(*b*). Here, the velocities are different, and the in-plane (with polarization $\mathbf{g}^{(2)} = \mathbf{e}_2$) transverse wave velocity is a function of the applied magnetic field, namely

$$\bar{c}_1 = \lambda^{-1/2}\sqrt{\bar{G}/\bar{\rho}} \quad \left(\mathbf{g}^{(1)} = \mathbf{e}_3\right) \tag{48}$$

and

$$\bar{c}_2 = \sqrt{\left(\lambda^{-1} + \lambda^2\left(\frac{\check{G}}{\bar{G}} - 1 - B_L^2\left(1 - \frac{\check{\mu}}{\bar{\mu}}\right)\right)\right)\frac{\bar{G}}{\bar{\rho}}} \quad \left(\mathbf{g}^{(2)} = \mathbf{e}_2\right) \tag{49}$$

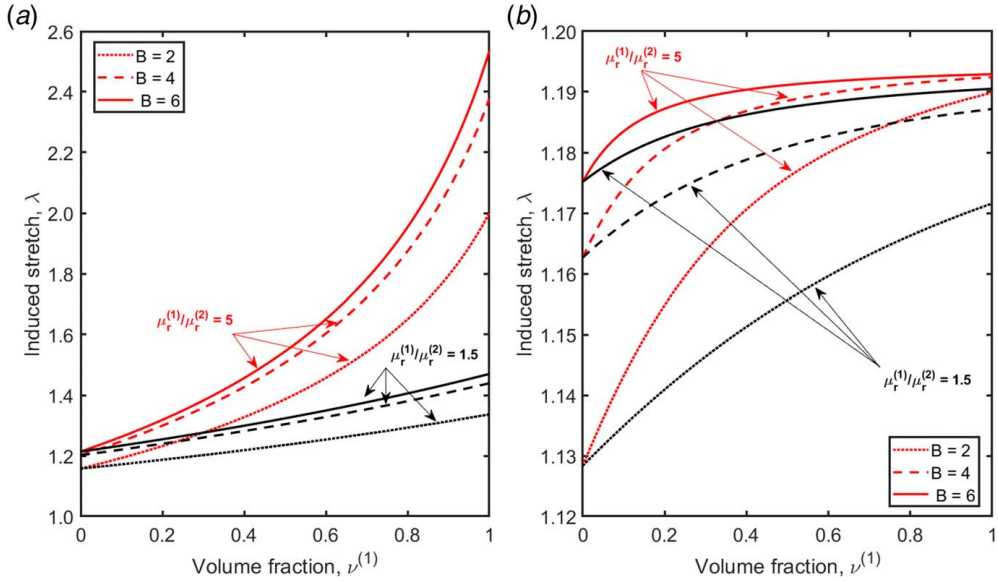

Fig. 3 Induced stretch versus volume fraction $\nu^{(1)}$ for laminates with (*a*) neo-Hookean phases and (*b*) Gent ($J_m = 0.1$); with two different ratios of $\mu_r^{(1)}/\mu_r^{(2)} = 1.5$ and 5 when $\mu_r^{(2)} = 1.5$. The dotted, dashed, and solid curves are for magnetic induction $B = 2$, 4, and 6, respectively.

Figure 5(*a*) shows the velocities of transverse waves given by Eqs. (47), (48), and (49) as functions of the dimensionless magnetic induction for the MAE composite with $\nu^{(1)} = 0.2$, $G^{(1)}/G^{(2)} = 1$, $G^{(2)} = 1$ MPa, $\mu_r^{(1)}/\mu_r^{(2)} = 5$, and $\mu_r^{(2)} = 1.5$ (such MAE laminates can be constructed from layers filled with a mixture of magnetically inactive and active stiff fillers, and from layers filled with magnetizable particles). The velocities are normalized by their corresponding values in the undeformed state (no deformation, nor magnetic excitation), $\bar{c}_0 = \bar{c}\,(B_L = 0)$. Consequently, the presented results are true for any choice in $\rho^{(1)}/\rho^{(2)}$. The solid and dashed-dotted curves are for the transverse wave velocity with the propagation direction parallel to the layers $\mathbf{n} = \mathbf{e}_1$ and polarizations $\mathbf{g}^{(2)} = \mathbf{e}_2$ and $\mathbf{g}^{(1)} = \mathbf{e}_1$, respectively. The dotted curve corresponds to the velocity of the transverse waves traveling in the direction normal to the laminates ($\mathbf{n} = \mathbf{e}_2$). The velocity increases slightly as the magnetic intensity level is magnified. For the transverse waves traveling along the layers, the magnetically induced changes result in a decrease in the velocity. The velocity of the out-of-plane wave experiences only slight reduction due to the induced deformation, while the in-plane wave ($\mathbf{g}^{(2)} = \mathbf{e}_2$) is affected significantly by the magnetic field.

Figure 5(*b*) shows the corresponding induced stretch versus Lagrangian magnetic induction, together with the limiting critical magnetic induction level and the corresponding induced stretch. Note that Eq. (49) produces the formula for the critical stretch and magnetic field at which the composite loses magnetomechanical stability [41]. Recall that this occurrence is identified with vanishing of the velocity value [28]. In particular, Eq. (49) yields

$$B_L^{(cr)} = \left(\lambda_{cr}^{-3} + \frac{\check{G}}{\bar{G}} - 1\right)^{1/2} \left(1 - \frac{\check{\mu}}{\bar{\mu}}\right)^{-1/2} \tag{50}$$

Moreover, substitution of Eq. (35) into Eq. (50) produces a polynomial equation for the critical stretch

$$a_5\,\lambda_{cr}^5 + a_3\,\lambda_{cr}^3 + a_2\,\lambda_{cr}^2 + 1 = 0 \tag{51}$$

where $a_5 = \bar{\mu}_r^{-1} - \check{G}(\bar{G}\,\check{\mu}_r)^{-1}$, $a_3 = \check{G}\bar{G}^{-1} - 1$, and $a_2 = -\bar{\mu}_r^{-1}$. For magnetically inactive laminates, the expression for the critical stretch reduces to

$$\lambda_{cr} = \left(1 - \frac{\check{G}}{\bar{G}}\right)^{-1/3} \tag{52}$$

recovering the result for the purely mechanical case [28]. Figure 6 illustrates the result for the critical magnetic field (Eq. (50)) showing the contour plots in the coordinates of shear modulus

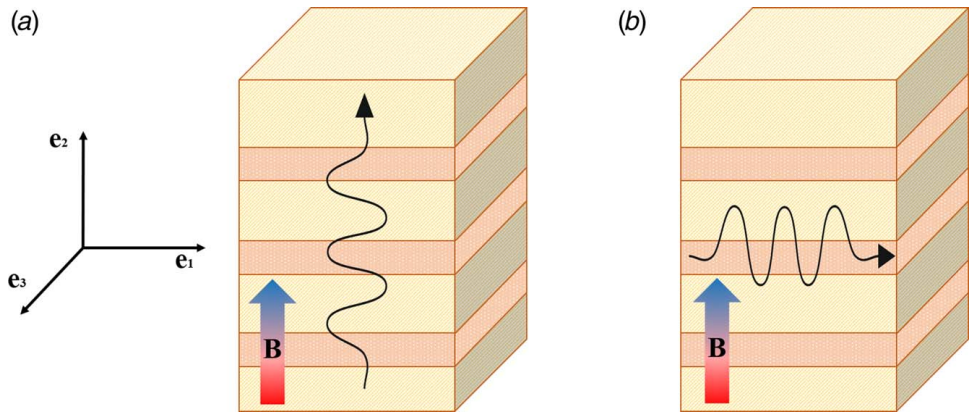

Fig. 4 Schematic representation of transverse waves traveling in the direction (*a*) normal and (*b*) parallel to layers

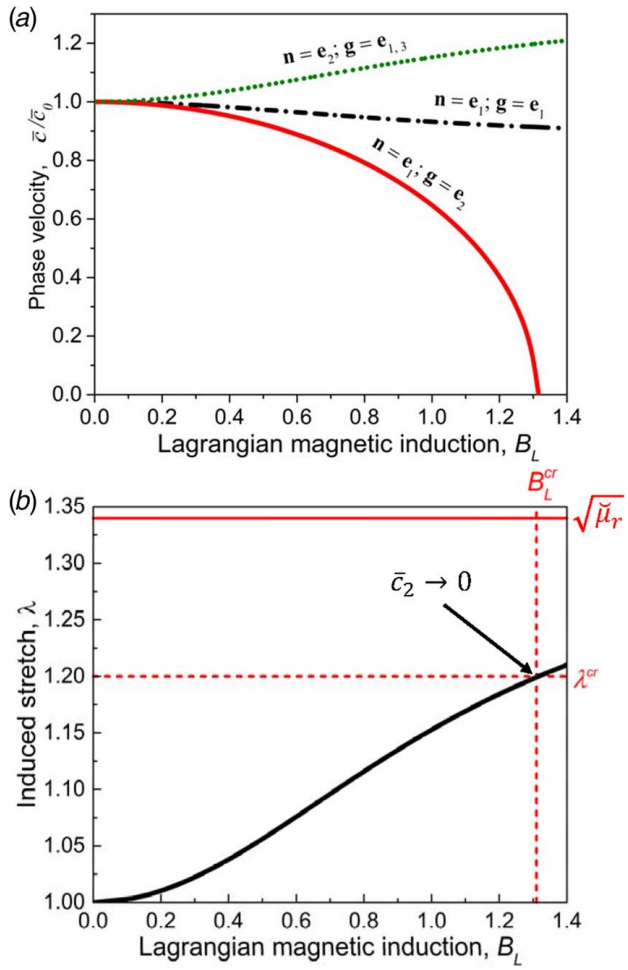

Fig. 5 (*a*) Velocities of transverse waves (Eqs. (47), (48), and (49)) as functions of the dimensionless magnetic induction for MAE layered materials with $\nu^{(1)} = 0.2$, $G^{(1)}/G^{(2)} = 1$, $G^{(2)} = 1$ MPa, $\mu_r^{(1)}/\mu_r^{(2)} = 5$, and $\mu_r^{(2)} = 1.5$ (*b*) stretch versus Lagrangian magnetic induction

and magnetic permeability ratios of the constituents. These results describe the behavior of the neo-Hookean magnetoactive laminates with $\nu^{(1)} = 0.5$ and $\rho^{(1)}/\rho^{(2)} = 1$. Two ranges of contrasts (*a*) $2\mu_r^{(1)}/\mu_r^{(2)}10$ and $2 \leqslant G^{(1)}/G^{(2)} \leqslant 20$ and (*b*) $1.1\mu_r^{(1)}/\mu_r^{(2)}2$ and $1 \leqslant G^{(1)}/G^{(2)} \leqslant 2$ are demonstrated separately.

3.2.3 Transverse Wave Propagation at Oblique Angles. Next, we consider oblique transverse wave propagating in the direction $\mathbf{n} = \cos\varphi\ \mathbf{e}_1 + \sin\varphi\ \mathbf{e}_2$. By combining the expressions for the velocities Eq. (46) with Eqs. (31) and (35), we obtain the slownesses plots $\bar{s}(\varphi) = 1/\bar{c}(\varphi)$ presented in Fig. 7 for (*a*) out-of-plane (with polarization $\mathbf{g} = \mathbf{e}_3$) and (*b*) in-plane (with polarization vector lying in plane $\langle \mathbf{e}_1, \mathbf{e}_2 \rangle$) transverse waves. The examples are given by the magnetoelastic composites of $\nu^{(1)} = 0.2$, $G^{(1)}/G^{(2)} = 1$, $\mu_r^{(1)}/\mu_r^{(2)} = 5$, $G^{(2)} = 1$ MPa, and $\mu_r^{(2)} = 1.5$ excited magnetically. These solid, dashed, and dotted curves correspond to the slownesses of the laminates subjected to the magnetic induction $B_L = 0$, 0.63, and 1.26, respectively. The out-of-plane wave velocity is weakly affected by the magnetic excitation. However, the in-plane transverse wave velocity experiences more pronounced changes as the magnetic induction is increased, especially as the direction of the wave propagation changes from the one perpendicular to the layers to the one along the layers. It can be seen from the elongated (along n_1-axis) elliptical shape of the slowness curve for the laminate subjected to $B_L = 1.26$, indicating that the velocity of the wave traveling along the layers significantly drops near a magnetoelastic instability.

3.3 Transverse Wave Band Gaps. Let us consider infinitesimal steady-state transverse excitations propagating perpendicularly to the layers (in x_2 or $\mathbf{e}_2$ direction, as shown in Fig. 1). We assume that the incremental fields $\mathbf{u}^{(\xi)}$, $\dot{\mathbf{B}}_{L\star}^{(\xi)}$, and $\dot{p}^{(\xi)}$ are functions of the coordinate x_2 and time t. The magnetoelastic tensors (Eq. (12)) for the energy-density function (Eq. (24)) are

$$\mathbb{C}_{ijkl}^{(\xi)} = 2\left(\delta_{ik}\, b_{lj}^{(\xi)}\psi_1^{(\xi)} + 2\, b_{ij}^{(\xi)} b_{kl}^{(\xi)}\psi_{11}^{(\xi)}\right) + \frac{1}{\mu^{(\xi)}}\delta_{ik}\, B_l^{(\xi)} B_j^{(\xi)},$$
$$\mathcal{B}_{ijk}^{(\xi)} = \frac{1}{\mu^{(\xi)}}\left(\delta_{ik}\, B_j^{(\xi)} + \delta_{jk}\, B_i^{(\xi)}\right), \quad \text{and} \quad M_{ij}^{(\xi)} = \frac{1}{\mu^{(\xi)}}\delta_{ij} \tag{53}$$

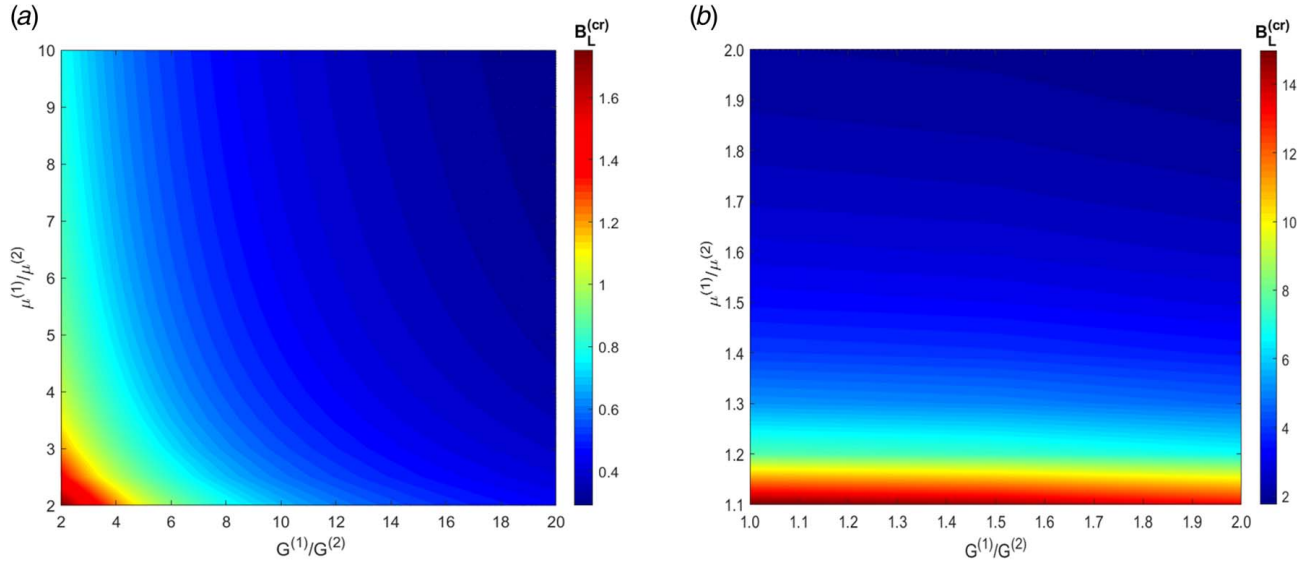

Fig. 6 The critical Lagrangian magnetic induction contour map as a function of contrasts in shear modulus and relative magnetic permeability of phases for neo-Hookean laminates of $\nu^{(1)} = 0.5$: (*a*) $2\mu_r^{(1)}/\mu_r^{(2)}10$ and $2 \leqslant G^{(1)}/G^{(2)} \leqslant 20$ (*b*) $1.1\mu_r^{(1)}/\mu_r^{(2)}$ 2 and $1 \leqslant G^{(1)}/G^{(2)} \leqslant 2$

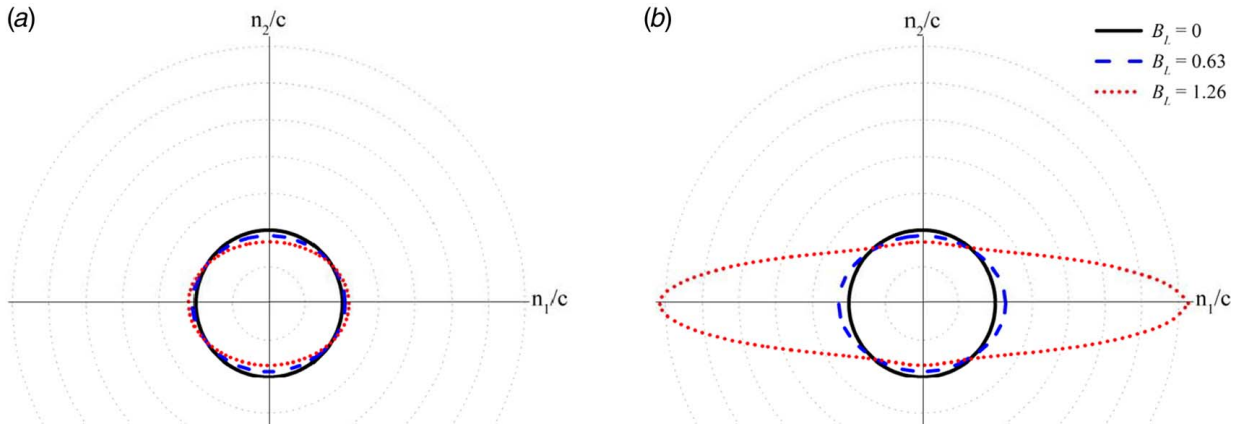

Fig. 7 Slowness curves for (*a*) the out-of-plane and (*b*) the in-plane transverse waves propagating in the magnetoelastic laminates with $\nu^{(1)}=0.2$, $G^{(1)}/G^{(2)}=1$, $\mu_r^{(1)}/\mu_r^{(2)}=5$, $G^{(2)}=1$ MPa and $\mu_r^{(2)}=1.5$ subjected to a magnetic field perpendicularly to the layers. Slowness is normalized by $c=\sqrt{\check{G}/\bar{\rho}}$. Scale is 0.5 per division. The vertical and horizontal axes with the labels $n_2/\bar{c}$ and $n_1/\bar{c}$ only indicate the principal directions and physical quantities presented on the polar plot.

where $\psi_1^{(\xi)}=\partial\psi^{(\xi)}/\partial I_1^{(\xi)}$ and $\psi_{11}^{(\xi)}=\partial\psi_1^{(\xi)}/\partial I_1^{(\xi)}$. As before, we assume the magnetically induced deformation gradient (Eq. (31)). Thus, substitution of Eqs. (13), (14), and (53) into Eq. (11) yields

$$\frac{\partial^2 u_1^{(\xi)}}{\partial t^2}=\left(c^{(\xi)}\right)^2\frac{\partial^2 u_1^{(\xi)}}{\partial x_2^2},\quad \frac{\partial\dot{p}^{(\xi)}}{\partial x_2}=0,\quad \text{and}\quad \frac{\partial^2 u_3^{(\xi)}}{\partial t^2}=\left(c^{(\xi)}\right)^2\frac{\partial^2 u_3^{(\xi)}}{\partial x_2^2} \tag{54}$$

where

$$c^{(\xi)}=\lambda\sqrt{2\psi_1^{(\xi)}/\rho^{(\xi)}} \tag{55}$$

Inserting Eqs. (14), (53), and (31) into Eq. (13) gives

$$\begin{aligned}
&\dot{P}_{\star 12}^{(\xi)}=2\,\lambda^2\,\psi_1^{(\xi)}\frac{\partial u_1^{(\xi)}}{\partial x_2}+\frac{B_2^{(\xi)}}{\mu^{(\xi)}}\left(B_2^{(\xi)}\frac{\partial u_1^{(\xi)}}{\partial x_2}+\dot{B}_{L\star 1}^{(\xi)}\right),\\
&\dot{H}_{L\star 1}^{(\xi)}=\frac{1}{\mu^{(\xi)}}\left(B_2^{(\xi)}\frac{\partial u_1^{(\xi)}}{\partial x_2}+\dot{B}_{L\star 1}^{(\xi)}\right)\dot{P}_{\star 22}^{(\xi)}=\frac{2}{\mu^{(\xi)}}B_2^{(\xi)}\dot{B}_{L\star 2}^{(\xi)}-\dot{p}^{(\xi)}\\
&\dot{P}_{\star 32}^{(\xi)}=2\,\lambda^2\,\psi_1^{(\xi)}\frac{\partial u_3^{(\xi)}}{\partial x_2}+\frac{B_2^{(\xi)}}{\mu^{(\xi)}}\left(B_2^{(\xi)}\frac{\partial u_3^{(\xi)}}{\partial x_2}+\dot{B}_{L\star 3}^{(\xi)}\right),\\
&\dot{H}_{L\star 3}^{(\xi)}=\frac{1}{\mu^{(\xi)}}\left(B_2^{(\xi)}\frac{\partial u_3^{(\xi)}}{\partial x_2}+\dot{B}_{L\star 3}^{(\xi)}\right)
\end{aligned} \tag{56}$$

where Eq. $(23)_2$ reduces to $B_2^{(\xi)}=B_2$.

The incremental interface conditions between the layers ($x_2=0$) read as

$$\begin{aligned}
&\dot{P}_{\star 12}^{(1)}=\dot{P}_{\star 12}^{(2)},\quad \dot{P}_{\star 22}^{(1)}=\dot{P}_{\star 22}^{(2)},\quad \dot{P}_{\star 32}^{(1)}=\dot{P}_{\star 32}^{(2)},\\
&\dot{H}_{L\star 1}^{(1)}=\dot{H}_{L\star 1}^{(2)},\quad \dot{H}_{L\star 3}^{(1)}=\dot{H}_{L\star 3}^{(2)},\quad \dot{B}_{L\star 2}^{(1)}=\dot{B}_{L\star 2}^{(2)}
\end{aligned} \tag{57}$$

Thus, inserting Eq. (56) into Eq. (57), we obtain

$$\begin{aligned}
&\psi_1^{(1)}\frac{\partial u_1^{(1)}}{\partial x_2}\bigg|_{x_2=0}=\psi_1^{(2)}\frac{\partial u_1^{(2)}}{\partial x_2}\bigg|_{x_2=0},\quad \psi_1^{(1)}\frac{\partial u_3^{(1)}}{\partial x_2}\bigg|_{x_2=0}=\psi_1^{(2)}\frac{\partial u_3^{(2)}}{\partial x_2}\bigg|_{x_2=0},\\
&\dot{p}^{(2)}-\dot{p}^{(1)}=B_2\,\dot{B}_{L\star 2}\left(\frac{1}{\mu^{(2)}}-\frac{1}{\mu^{(1)}}\right)
\end{aligned} \tag{58}$$

We seek a solution for Eq. $(54)_1$ in the following form:

$$u_1^{(\xi)}=M^{(\xi)}e^{i\left(k^{(\xi)}x_2-\omega t\right)}+N^{(\xi)}e^{i\left(-k^{(\xi)}x_2-\omega t\right)} \tag{59}$$

where $k^{(\xi)}=\omega/c^{(\xi)}$ is the wavenumber and ω is the angular frequency. Perfect bonding between the layers entails

$$u_1^{(1)}\big|_{x_2=0}=u_1^{(2)}\big|_{x_2=0} \tag{60}$$

Next, inserting Eq. (59) into Eq. (60), we obtain

$$M^{(1)}+N^{(1)}-M^{(2)}-N^{(2)}=0 \tag{61}$$

Substituting Eq. (59) into Eq. $(58)_1$, we have

$$\frac{\psi_1^{(1)}}{c^{(1)}}M^{(1)}-\frac{\psi_1^{(1)}}{c^{(1)}}N^{(1)}-\frac{\psi_1^{(2)}}{c^{(2)}}M^{(2)}+\frac{\psi_1^{(2)}}{c^{(2)}}N^{(2)}=0 \tag{62}$$

Two more relations for constants $M^{(1)}$, $N^{(1)}$, $M^{(2)}$, and $N^{(2)}$ can be derived from the periodicity of the laminate. To this end, the form of the solution (Eq. (59)) is altered to be the steady-state wave with the same wavenumber k for both layers

$$u_1^{(\xi)}=U_1^{(\xi)}(x_2)e^{i(kx_2-\omega t)} \tag{63}$$

where

$$U_1^{(\xi)}(x_2)=M^{(\xi)}e^{iK_-^{(\xi)}x_2}+N^{(\xi)}e^{-iK_+^{(\xi)}x_2}\quad\text{and}\quad K_\pm^{(\xi)}=k^{(\xi)}\pm k \tag{64}$$

In accordance with the Floquet theorem, functions $U_1^{(\xi)}(x_2)$ must be periodic with $l=l^{(1)}+l^{(2)}$ (Fig. 1(*b*)), i.e.,

$$U_1^{(1)}(-l^{(1)})=U_1^{(2)}(l^{(2)}) \tag{65}$$

Then, inserting Eq. (64) into Eq. (65) gives

$$e^{-iK_-^{(1)}l^{(1)}}M^{(1)}+e^{iK_+^{(1)}l^{(1)}}N^{(1)}-e^{iK_-^{(2)}l^{(2)}}M^{(2)}-e^{-iK_+^{(2)}l^{(2)}}N^{(2)}=0 \tag{66}$$

Next, substituting Eq. (63) and $\dot{B}_{L\star 1}^{(\xi)}=h_1^{(\xi)}(x_2)e^{i(kx_2-\omega t)}$ into Eq. $(56)_1$, we obtain

$$\begin{aligned}
&\dot{H}_{L\star 1}^{(\xi)}(x_2,t)=\mathcal{H}_1^{(\xi)}(x_2)e^{i(kx_2-\omega t)},\quad\text{and}\\
&\mathcal{H}_1^{(\xi)}(x_2)=\frac{1}{\mu^{(\xi)}}\left(B_2\frac{i\omega}{c^{(\xi)}}\left(M^{(\xi)}e^{iK_-^{(\xi)}x_2}-N^{(\xi)}e^{-iK_+^{(\xi)}x_2}\right)+h_1^{(\xi)}(x_2)\right)
\end{aligned} \tag{67}$$

and

$$\dot{P}^{(\xi)}_{\star 12}(x_2,\, t) = \mathcal{P}^{(\xi)}_1(x_2) e^{i(kx_2 - \omega t)}, \quad \text{and}$$

$$\mathcal{P}^{(\xi)}_1(x_2) = 2\ \lambda_2{}^2\ \psi^{(\xi)}_1 \frac{i\omega}{c^{(\xi)}} \left(M^{(\xi)} e^{iK^{(\xi)}_- x_2} - N^{(\xi)} e^{-iK^{(\xi)}_+ x_2} \right) + B_2 \mathcal{H}^{(\xi)}_1(x_2) \tag{68}$$

where according to the Floquet theorem

$$\begin{aligned} &\mathcal{P}^{(1)}_1(-l^{(1)}) = \mathcal{P}^{(2)}_1(l^{(2)}), \quad \mathcal{H}^{(1)}_1(-l^{(1)}) = \mathcal{H}^{(2)}_1(l^{(2)}), \\ &h^{(1)}_1(-l^{(1)}) = h^{(2)}_1(l^{(2)}) \end{aligned} \tag{69}$$

Finally, combining Eq. (68) and Eq. (69), we obtain

$$\begin{aligned} &\frac{\psi^{(1)}_1}{c^{(1)}} e^{-iK^{(1)}_- l^{(1)}} M^{(1)} - \frac{\psi^{(1)}_1}{c^{(1)}} e^{iK^{(1)}_+ l^{(1)}} N^{(1)} - \frac{\psi^{(2)}_1}{c^{(2)}} e^{iK^{(2)}_- l^{(2)}} M^{(2)} \\ &+ \frac{\psi^{(2)}_1}{c^{(2)}} e^{-iK^{(2)}_+ l^{(2)}} N^{(2)} = 0 \end{aligned} \tag{70}$$

The condition for the existence of a nontrivial solution for the system of Eqs. (61), (62), (66), and (70) is

$$\det \begin{bmatrix} 1 & 1 & -1 & -1 \\ \frac{\psi^{(1)}_1}{c^{(1)}} & -\frac{\psi^{(1)}_1}{c^{(1)}} & -\frac{\psi^{(2)}_1}{c^{(2)}} & \frac{\psi^{(2)}_1}{c^{(2)}} \\ e^{-iK^{(1)}_- l^{(1)}} & e^{iK^{(1)}_+ l^{(1)}} & -e^{iK^{(2)}_- l^{(2)}} & -e^{-iK^{(2)}_+ l^{(2)}} \\ \frac{\psi^{(1)}_1}{c^{(1)}} e^{-iK^{(1)}_- l^{(1)}} & -\frac{\psi^{(1)}_1}{c^{(1)}} e^{iK^{(1)}_+ l^{(1)}} & -\frac{\psi^{(2)}_1}{c^{(2)}} e^{iK^{(2)}_- l^{(2)}} & \frac{\psi^{(2)}_1}{c^{(2)}} e^{-iK^{(2)}_+ l^{(2)}} \end{bmatrix} = 0 \tag{71}$$

Remarkably, after some mathematical manipulations with Eq. (71) and taking into account Eq. (55), we can finally obtain the following compact relation:

$$\begin{aligned} \cos kl = &\cos\left(\frac{\omega\ l^{(1)}}{c^{(1)}}\right) \cos\left(\frac{\omega\ l^{(2)}}{c^{(2)}}\right) - \frac{1}{2}\left(\frac{\rho^{(1)} c^{(1)}}{\rho^{(2)} c^{(2)}} + \frac{\rho^{(2)} c^{(2)}}{\rho^{(1)} c^{(1)}}\right) \\ &\times \sin\left(\frac{\omega\ l^{(1)}}{c^{(1)}}\right) \sin\left(\frac{\omega\ l^{(2)}}{c^{(2)}}\right) \end{aligned} \tag{72}$$

defining the dispersion relation $\omega = \omega(k)$. Here, $c^{(\xi)}(\lambda)$ and $l^{(\xi)}(\lambda)$ are functions of deformation; in particular, the dependence of the velocity on deformation can be found from Eq. (55). Thus, for instance, for Gent model, substitution of Eq. (38) into Eq. (55) yields

$$c_G{}^{(\xi)} = \lambda \left(\frac{J_m{}^{(\xi)}}{3 + J_m{}^{(\xi)} - \lambda^2 - 2\lambda^{-1}} \frac{\mu^{(\xi)}}{\rho^{(\xi)}} \right)^{1/2} \tag{73}$$

The deformation of the laminate results in the layer thickness change given by Eq. (18). Equations (39), (73), (18), and (72) allow to evaluate dispersion relations for transverse waves propagating perpendicularly to the layers in magnetoelastic layered materials subjected to a magnetic field perpendicularly to the layers. Figure 8 illustrates a dispersion relation Eq. (72) for the MAE laminate with Gent phases having $J_m = 0.1$, $\nu^{(1)} = 0.25$, $G^{(1)}/G^{(2)} = \mu^{(1)}_r/\mu^{(2)}_r = 15$, and $\rho^{(1)}/\rho^{(2)} = 1$ that is subjected to the magnetic field of magnitude $B_L = 2$ (the corresponding induced stretch is $\lambda = 1.17$). The reported frequency is normalized as $f_n = (\omega L/2\pi)\sqrt{\bar{\rho}/\breve{G}}$. The dispersion relation has several frequency ranges where transverse waves are not allowed to propagate, i.e., band gaps, denoted by the shaded areas. The lowest band gap is induced around the mid-gap Bragg frequency that can be evaluated directly from the diagram in Fig. 8(*a*) as the intersection of a tangent to the fundamental mode around the origin and the Brillouin zone boundary at $\mathrm{Re}(kl/2\pi) = 0.5$. This fact together with the smooth variations of the imaginary parts of the dispersion bands (Fig. 8(*b*)) point out at the Bragg scattering origin of the band gap mechanism [42,43].

The derived dispersion relation is in total agreement with the exact solution for long transverse waves Eq. (47) traveling perpendicularly to the layers in magnetoelastic layered media. This confirms that the transverse wave propagation does not depend on a magnetic field for this specific setting, and the dispersion curves can be tuned by the application of a magnetic field only through induced deformation. Equation (72) mimics the classical result for purely elastic layered materials [44] in the absence of magnetically or mechanically induced deformations. We note that this relation is identical to the one studied by Galich et al. [28] for the purely elastic problem, and it is also identical to the dispersion relation for the electroactive layered materials, which was first derived by Galich and Rudykh [29] and, more recently, by Jandron and Henann [45], who also validated the result numerically. Moreover, the derived dispersion relation coincides with the finite element simulations in the purely mechanical case (in the absence of a magnetic field) [46,47]. Here, however, the deformation is induced by a magnetic field. The applied magnetic stimulus leads to an extension (in the magnetic field direction) of the composites, whereas the electric excitation produces contraction (in the field direction). Next, we illustrate how the transverse wave band gaps change with the induced deformation due to the application of a magnetic field. Figure 9 shows the transverse wave band gap width change with an increase in the Lagrangian magnetic induction applied perpendicularly to the layers in the MAE laminates with Gent magnetoelastic phases. The examples are given for the laminates with the $\nu^{(1)} = 0.15$, $G^{(1)}/G^{(2)} = \mu^{(1)}_r/\mu^{(2)}_r = 50$, $\mu^{(2)}_r = 1.5$, $\rho^{(1)}/\rho^{(2)} = 1$, and $J_m = 0.1$. Clearly, the magnetic field widens and shifts transverse wave band gaps up toward higher frequencies. For instance, the applied $B_L = 1.5$ to the laminate shifts the lower boundary of the first transverse band gap from $f_n = 0.47$ up to 0.71 and widens it

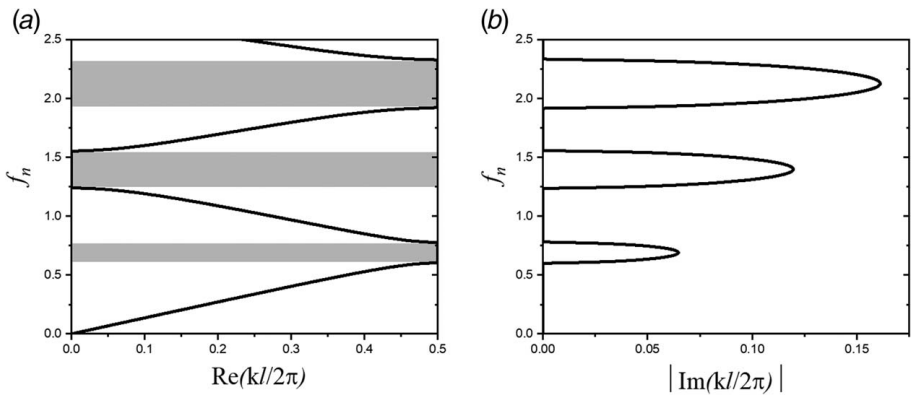

Fig. 8 Dispersion diagrams for (*a*) real part and (*b*) imaginary part for transverse waves in Gent laminate with $J_m = 0.1$, $\nu^{(1)} = 0.25$, $G^{(1)}/G^{(2)} = \mu^{(1)}_r/\mu^{(2)}_r = 15$, and $\rho^{(1)}/\rho^{(2)} = 1$. The magnetic field of $B_L = 2$ is applied to the laminate. The shaded rectangles refer to the transverse wave band gaps. Frequency is normalized as $f_n = (\omega L/2\pi)\sqrt{\bar{\rho}/\breve{G}}$.

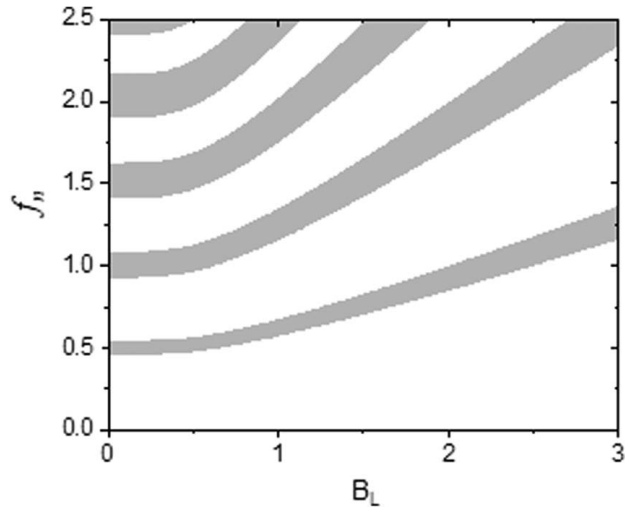

Fig. 9 Band gap widths versus magnetic induction in Gent layered materials with $J_m = 0.1$, $\nu^{(1)} = 0.15$, and $\mu_r^{(1)}/\mu_r^{(2)} = G^{(1)}/G^{(2)} = 50$

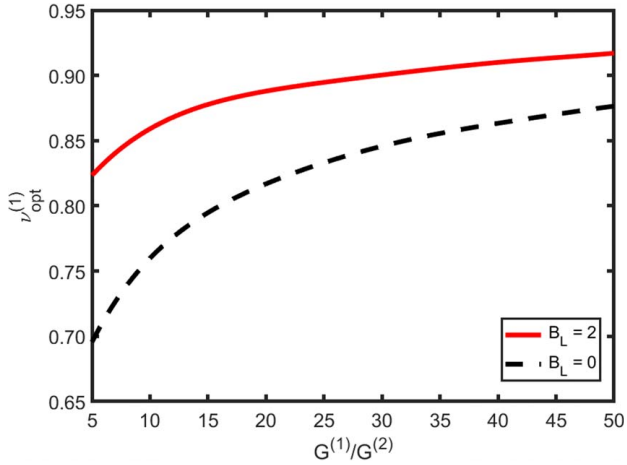

Fig. 11 The optimum volume fraction; $\nu^{(1)}$ versus the stiffness ratio (shear modulus); $G^{(1)}/G^{(2)}$ in Gent layered materials with $J_m = 0.1$, $G^{(2)} = 1$ MPa, $\mu_r^{(1)}/\mu_r^{(2)} = 50$, and $\rho^{(1)}/\rho^{(2)} = 1$. The dashed and solid curves are for the magnetic field of $B_L = 0$ and $B_L = 2$, respectively.

from $\Delta f_n = 0.07$ up to 0.12 (see Fig. 9). Figure 10 displays the lowest (first) band gap width versus the volume fraction in Gent layered materials with $J_m = 0.1$, $\mu_r^{(1)}/\mu_r^{(2)} = 5$, and $G^{(1)}/G^{(2)} = 10$. The light and dark gray areas represent the lowest band gap width of the composite without magnetic excitation ($B_L = 0$) and excited by $B_L = 1.25$. One can see that in accordance with the previous observations the magnetic excitation widens the band gap width. The band gap width reaches a maximum at a certain volume fraction, in particular, $\nu_m^{(1)} = 0.76$ for the considered composition; the band gap width changes from $\Delta f_n^{(\max)} = 0.406$ at $B_L = 0$, to $\Delta f_n^{(\max)} = 0.494$ when excited magnetically by $B_L = 1.25$; in addition, the upper boundary attains the frequency of $f_n^{(up)} = 0.96$ (at $B_L = 1.25$) in comparison to $f_n^{(up)} = 0.79$ ($B_L = 0$). We remark, however, that the optimum volume fraction value (for which the maximum width is observed) barely changes with the magnetic excitation.

Finally, to provide the guidelines for designing wide low frequency band gaps, we show how the optimum volume fraction value changes with the stiffness ratio and the relative magnetic permeability. Figure 11 shows the optimum volume fraction versus the stiffness ratio $G^{(1)}/G^{(2)}$ when $\mu_r^{(1)}/\mu_r^{(2)} = 50$, $J_m = 0.1$, $G^{(2)} = 1$ MPa, $\mu_r^{(2)} = 1.5$, and $\rho^{(1)}/\rho^{(2)} = 1$. The dashed and solid curves represent the composite without magnetic excitation and magnetically excited ($B_L = 2$) composite, respectively. The results show that the value of the optimum concentration of the stiff layers increases as the stiffness ratio is increased; also, the difference between these values becomes smaller. This is because the level of the induced deformation decreases for composites with high stiffness of the reinforcing layers (when immersed into a magnetic field of the same level).

Figure 12 displays the optimum volume fraction versus the relative magnetic permeability for the composite with $G^{(1)}/G^{(2)} = 50$. Obviously, the optimum value does not change for the undeformed composite (dashed horizontal line for $B_L = 0$), however, a slight increase in the optimum concentration is observed for the excited composite (solid curve for $B_L = 2$). For instance, the optimum volume fraction of the stiff layers increases from about 0.88 for $\mu_r^{(1)}/\mu_r^{(2)} = 1$ to 0.917 for the composite with high contrast in magnetic properties of the constituents $\mu_r^{(1)}/\mu_r^{(2)} = 50$.

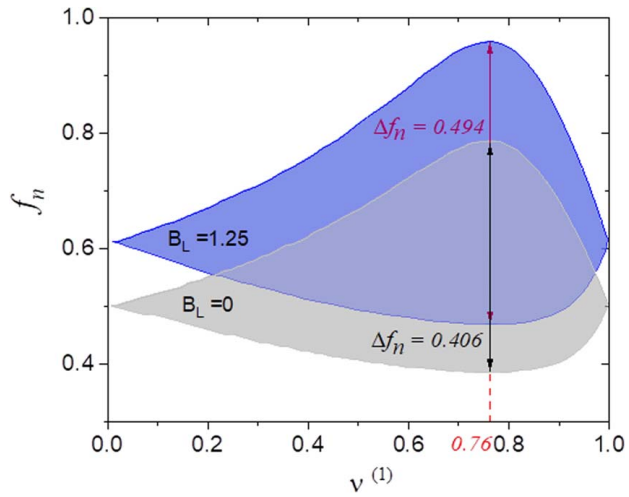

Fig. 10 The first (lowest) band gap widths versus volume fraction in Gent layered materials with $J_m = 0.1$, $\mu_r^{(1)}/\mu_r^{(2)} = 5$, and $G^{(1)}/G^{(2)} = 10$ (Color version online.)

4 Conclusion

We investigated the behavior of periodic laminates with magnetoactive hyperelastic isotropic phases. First, we derived explicit

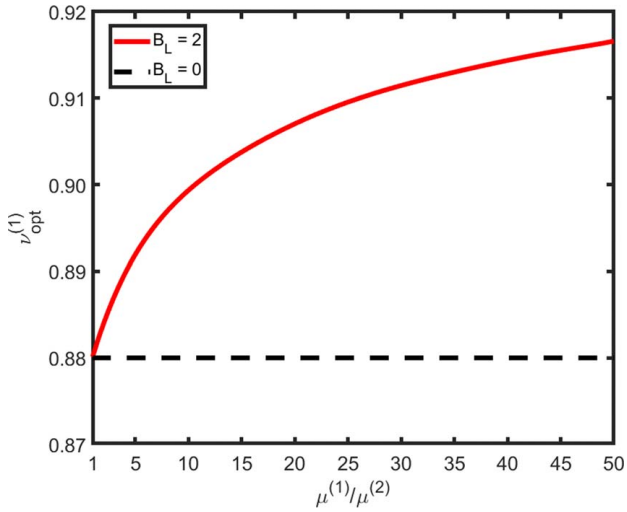

Fig. 12 The optimum volume fraction; $\nu^{(1)}$ versus the relative magnetic permeability; $\mu_r^{(1)}/\mu_r^{(2)}$ in Gent layered materials with $J_m = 0.1$, $\mu_r^{(2)} = 1.5$, $G^{(1)}/G^{(2)} = 50$, and $\rho^{(1)}/\rho^{(2)} = 1$. The dashed and solid curves are for the magnetic field of $B_L = 0$ and $B_L = 2$, respectively.

expressions for the magnetically induced stretch developing in response to a remotely applied magnetic field. The relations between the induced stretch and applied magnetic field were derived for laminates with neo-Hookean and Gent magnetoactive phases. Second, the exact solution for magnetoactive laminates was used to construct the homogenized effective energy function and to derive the explicit expressions for transverse wave velocities as functions of the applied magnetic field, deformation, and wave propagation direction. In general, one of the two transverse wave velocities depends explicitly on the applied magnetic field. However, for the specific case of the transverse waves propagating perpendicularly to the layers, the velocities of both transverse waves are independent of an applied magnetic field. However, the transverse wave velocities still can be tuned through the magnetically induced deformation. Based on the long wave analysis for the case of transverse waves propagating along the layers, we derived the explicit expressions for the critical magnetic field corresponding to the onset of macroscopic or long wave instabilities. The critical condition was specified for the deformation induced by a remotely applied magnetic field. Finally, we studied the transverse wave dispersion relations in the magnetoactive laminates. Similarly to purely mechanical laminates, the magnetoactive laminates possess forbidden frequency ranges or band gaps for transverse waves propagating perpendicularly to the layers. The transverse wave band gaps in neo-Hookean magnetoactive laminates are indifferent to the applied magnetic field and induced deformation. However, the pronounced stiffening effect of Gent magnetoactive laminates results in tunability of the transverse wave band gaps by the magnetically induced deformation. Thus, the width and position of the transverse wave band gaps can be controlled by a remotely applied magnetic field. The optimum volume fractions maximizing the lowest band gap were obtained to provide the guidelines toward the design of low frequency band gap magnetoactive materials.

References

[1] Ginder, J. M., Clark, S. M., Schlotter, W. F., and Nichols, M. E., 2002, "Magnetostrictive Phenomena in Magnetorheological Elastomers," Int. J. Mod. Phys. B, **16**(17n18), pp. 2412–2418.

[2] Guan, X., Donga, X., and Ou, J., 2008, "Magnetostrictive Effect of Magnetorheological Elastomer," J. Magn. and Magn. Mat., **320**(3–4), pp. 158–163.

[3] Varga, Z., Filipcsei, G., and Zrinyi, M., 2005, "Smart Composites with Controlled Anisotropy," Polymer, **46**(18), pp. 7779–7787.

[4] Ginder, J. M., Nichols, M. E., Elie, L. D., and Clark, S. M., 2000, "Controllable-Stiffness Components Based on Magnetorheological Elastomers," Proc. SPIE, **3985**(1), p. 418.

[5] Erb, R. M., Libanori, R., Rothfuchs, N., and Studart, A. R., 2012, "Composites Reinforced in Three Dimensions by Using Low Magnetic Fields," Science, **335**(6065), pp. 199–204.

[6] Ginder, J. M., Schlotter, W. F., and Nichols, M. E., 2001, "Magnetorheological Elastomers in Tunable Vibration Absorbers," Proc. SPIE, **4331**(1), pp. 103–111.

[7] Deng, H. X., Gong, X. L., and Wang, L. H., 2006, "Development of an Adaptive Tuned Vibration Absorber with Magnetorheological Eastomer," Smart Mater. Struct., **15**(5), pp. N111–N116.

[8] Wang, Q., Dong, X., Li, L., and Ou, J., 2018, "Mechanical Modeling for Magnetorheological Elastomer Isolators Based on Constitutive Equations and Electromagnetic Analysis," Smart Mater. Struct., **27**(6), p. 065017.

[9] Gong, X., Fan, Y., Xuan, S., Xu, Y., and Peng, C., 2012, "Control of the Damping Properties of Magnetorheological Elastomers by Using Polycaprolactone as a Temperature-Controlling Component," Ind. Eng. Chem. Res., **51**(18), pp. 6395–6403.

[10] Yang, J., Gong, X., Deng, H., Qin, L., and Xuan, S., 2012, "Investigation on the Mechanism of Damping Behavior of Magnetorheological Elastomers," Smart Mater. Struct., **21**(12), p. 125015.

[11] Farshad, M., and Le Roux, M., 2004, "A New Active Noise Abatement Barrier System," Polym. Test., **23**(7), pp. 855–860.

[12] Yu, K., Fang, N. X., Huang, G., and Wang, Q., 2018, "Magnetoactive Acoustic Metamaterials," Adv. Mater., **30**(21), pp. 1–10.

[13] Tian, T. F., Li, W. H., and Deng, Y. M., 2011, "Sensing Capabilities of Graphite Based MR Elastomers," Smart Mater. Struct., **20**(2), p. 025022.

[14] Lanotte, L., Ausanio, G., Hison, C., Iannotti, V., and Luponio, C., 2003, "The Potentiality of Composite Elastic Magnets as Novel Materials for Sensors and Actuators," Sens. Actuat., **106**(1–3), pp. 56–60.

[15] Kim, Y., Yuk, H., Zhao, R., Chester, S. A., and Zhao, X., 2018, "Printing Ferromagnetic Domains for Untethered Fast-Transforming Soft Materials," Nature, **558**(7709), pp. 274–279.

[16] Tang, S. Y., Zhang, X., Sun, S., Yuan, D., Zhao, Q., Yan, S., Deng, L., Yun, G., Zhang, J., Zhang, S., and Li, W., 2018, "Versatile Microfluidic Platforms Enabled by Novel Magnetorheological Elastomer Microactuators," Adv. Funct. Mater., **28**(8), p. 1705484.

[17] Stanier, D. C., Ciambella, J., and Rahatekar, S. S., 2016, "Fabrication and Characterisation of Short Fibre Reinforced Elastomer Composites for Bending and Twisting Magnetic Actuation," Compos. Part A, **91**(1), pp. 168–176.

[18] Makarova, L. A., Alekhina, Y. A., Rusakova, T. S., and Perov, N. S., 2016, "Tunable Properties of Magnetoactive Elastomers for Biomedical Applications," Phys. Procedia, **82**(1), pp. 38–45.

[19] Luo, Z., Evans, B. A., and Chang, C. H., 2019, "Magnetically Actuated Dynamic Iridescence Inspired by the Neon Tetra," ACS Nano, **13**(4), pp. 4657–4666.

[20] Tang, J., Qiao, Y., Chu, Y., Tong, Z., Zhou, Y., Zhang, W., Xie, S., Hu, J., and Wang, T., 2019, "Magnetic Double-Network Hydrogels for Tissue Hyperthermia and Drug Release," J. Mater. Chem. B, **7**(8), pp. 1311–1321.

[21] Maugin, G. A., 1981, "Wave Motion in Magnetizable Deformable Solids," Int. J. Eng. Sci., **19**(3), pp. 321–388.

[22] Abd-Alla, A. E. N., and Maugin, G. A., 1987, "Nonlinear Magnetoacoustic Equations," J. Acoust. Soc. Am., **82**(5), pp. 1746–1752.

[23] Hefni, I. A. Z. , Ghaleb, A. F. , and Maugin, G. A., 1995, "Surface Waves in a Nonlinear Magnetoelastic Conductor of Finite Electric Conductivity," Int. J. Eng. Sci., **33**(14), pp. 2085–2102.

[24] Boulanger, P., 1989, "Inhomogeneous Magnetoelastic Planewaves," North-Holland Ser. Appl. Math. Mech., **35**(C), pp. 601–606.

[25] Destrade, M., and Ogden, R. W., 2011, "On Magneto-acoustic Waves in Finitely Deformed Elastic Solids," Math. Mech. Solids, **16**(6), pp. 594–604.

[26] Saxena, P., and Ogden, R. W., 2011, "On Surface Waves in a Finitely Deformed Magnetoelastic Half-Space," Int. J. Appl. Mech., **3**(4), pp. 633–665.

[27] Saxena, P., and Ogden, R. W., 2012, "On Love-Type Waves in a Finitely Deformed Magnetoelastic Layered Half-Space," Z. Angew. Math. Phys., **63**(6), pp. 1177–1200.

[28] Galich, P. I., Fang, N. X., Boyce, M. C., and Rudykh, S., 2017, "Elastic Wave Propagation in Finitely Deformed Layered Materials," J. Mech. Phys. Solids, **98**(1), pp. 390–410.

[29] Galich, P. I., and Rudykh, S., 2017, "Shear Wave Propagation and Band Gaps in Finitely Deformed Dielectric Elastomer Laminates: Long Wave Estimates and Exact Solution," ASME J. Appl. Mech., **84**(9), p. 091002.

[30] Rudykh, S., and Bertoldi, K., 2013, "Stability of Anisotropic Magnetorheological Elastomers in Finite Deformations: A Micromechanical Approach.," J. Mech. Phys. Solids, **61**(4), pp. 949–967.

[31] Danas, K., Kankanala, S. V., and Triantafyllidis, N., 2012, "Experiments and Modeling of Iron-Particle-Filled Magnetorheological Elastomers," J. Mech. Phys. Solids, **60**(1), pp. 120–138.

[32] Galipeau, E., Rudykh, S., deBotton, G., and Castañeda, P. P., 2014, "Magnetoactive Elastomers with Periodic and Random Microstructures," Int. J. Solids Struct., **51**(18), pp. 3012–3024.

[33] Metsch, P., Kalina, K. A., Spieler, C., and Kästner, M., 2016, "A Numerical Study on Magnetostrictive Phenomena in Magnetorheological Elastomers," Comput. Mater. Sci., **124**(1), pp. 364–374.

[34] Vu, D. K., and Steinmann, P., 2007, "Nonlinear Electro-and Magneto-Elastostatics: Material and Spatial Settings," Int. J. Solids Struct., **44**(24), pp. 7891–7905.

[35] Keip, M. A., and Rambausek, M., 2016, "A Multiscale Approach to the Computational Characterization of Magnetorheological Elastomers," Int. J. Numer. Methods Eng., **107**(4), pp. 338–360.

[36] Keip, M. A., and Rambausek, M., 2017, "Computational and Analytical Investigations of Shape Effects in the Experimental Characterization of Magnetorheological Elastomers," Int. J. Solids Struct., **121**(1), pp. 1–20.

[37] Dorfmann, L., and Ogden, R. W., 2014, *Nonlinear Theory of Electroelastic and Magnetoelastic Interactions*, vol. 1, Springer, Boston, MA.

[38] Kankanala, S. V., and Triantafyllidis, N., 2008, "Magnetoelastic Buckling of a Rectangular Block in Plane Strain," J. Mech. Phys. Solids, **56**(4), pp. 1147–1169.

[39] Arruda, E. M., and Boyce, M. C., 1993, "A Three-Dimensional Constitutive Model for the Large Stretch Behavior of Rubber Elastic Materials," J. Mech. Phys. Solids, **41**(2), pp. 389–412.

[40] Gent, A. N., 1996, "A New Constitutive Relation for Rubber," Rubber Chem. Technol., **69**(1), pp. 59–61.

[41] Goshkoderia, A., and Rudykh, S., 2017, "Stability of Magnetoactive Composites with Periodic Microstructures Undergoing Finite Strains in the Presence of a Magnetic Field," Compos. Part B: Eng., **128**(1), pp. 19–29.

[42] Yuan, B., Humphrey, V. F., Wen, J., and Wen, X., 2013, "On the Coupling of Resonance and Bragg Scattering Effects in Three-Dimensional Locally Resonant Sonic Materials," Ultrasonics, **53**(7), pp. 1332–1343.

[43] Krushynska, A., Miniaci, M., Bosia, F., and Pugno, N., 2017, "Coupling Local Resonance with Bragg Band Gaps in Single-Phase Mechanical Metamaterials," Extreme Mech. Lett., **12**(1), pp. 30–36.

[44] Rytov, S., 1956, "Acoustical Properties of a Thinly Laminated Medium," Soviet Phys. Acoustics, **2**(1), pp. 68–80.

[45] Jandron, M., and Henann, D. L., 2018, "A Numerical Simulation Capability for Electroelastic Wave Propagation in Dielectric Elastomer Composites: Application to Tunable Soft Phononic Crystals," Int. J. Solids. Struct., **150**(1), pp. 1–21.

[46] Li, J., Slesarenko, V., Galich, P. I., and Rudykh, S., 2018, "Oblique Shear Wave Propagation in Finitely Deformed Layered Composites," Mech. Res. Commun., **87**(1), pp. 21–28.

[47] Slesarenko, V., Galich, P. I., Li, J., Fang, N. X., and Rudykh, S., 2018, "Foreshadowing Elastic Instabilities by Negative Group Velocity in Soft Composites," Appl. Phys. Lett., **113**(3), p. 031901.